RESEARCH ARTICLE

PROTEIN TARGETING

The principle of antagonism ensures protein targeting specificity at the endoplasmic reticulum

Martin Gamerdinger,[1] Marie Anne Hanebuth,[1] Tancred Frickey,[2] Elke Deuerling[1]*

The sorting of proteins to the appropriate compartment is one of the most fundamental cellular processes. We found that in the model organism *Caenorhabditis elegans*, correct cotranslational endoplasmic reticulum (ER) transport required the suppressor activity of the nascent polypeptide-associated complex (NAC). NAC did not affect the accurate targeting of ribosomes to ER translocons mediated by the signal recognition particle (SRP) pathway but inhibited additional unspecific contacts between ribosomes and translocons by blocking their autonomous binding affinity. NAC depletion shortened the life span of *Caenorhabditis elegans*, caused global mistargeting of translating ribosomes to the ER, and provoked incorrect import of mitochondrial proteins into the ER lumen, resulting in a strong impairment of protein homeostasis in both compartments. Thus, the antagonistic targeting activity of NAC is important in vivo to preserve the robustness and specificity of cellular protein-sorting routes.

In eukaryotes, a substantial fraction of membrane and secretory proteins are cotranslationally delivered to and translocated across the endoplasmic reticulum (ER) membrane. This transport is mediated by the signal recognition particle (SRP), which binds to hydrophobic signal sequence–containing ribosome-nascent chain complexes (RNCs) and targets them to the Sec61 translocon via the ER membrane-located SRP receptor (SR) (*1*–*6*). However, despite decades of research on SRP-mediated ER targeting, key questions regarding the requirement of additional sorting factors to guarantee accuracy and efficiency of protein transport remained unanswered. One early study discovered that an abundant protein complex termed nascent polypeptide-associated complex (NAC) may be required to prevent SRP from interaction with signal-less RNCs (*7*). This idea has been highly controversial, and the function of NAC in protein targeting, if any, remains unclear. Furthermore, ribosomes show a SRP-independent, high intrinsic affinity for Sec61 in vitro. This raises the question about the identity and the functional importance of a potential negative regulator that prevents unspecific ribosome-translocon interactions to ensure correct RNC sorting in vivo (*8*–*12*).

We used the metazoan *Caenorhabditis elegans* to dissect the factors underlying ER targeting specificity in vivo.

[1]Department of Biology, Institute of Molecular Microbiology, University of Konstanz, 78457 Konstanz, Germany.
[2]Department of Biology, Applied Bioinformatics Laboratory, University of Konstanz, 78457 Konstanz, Germany.
*Corresponding author. E-mail: elke.deuerling@uni-konstanz.de

NAC depletion shortens life span and induces ER and mitochondrial stress in *C. elegans*

To understand the potential role of the ribosome-associated α,β-heterodimeric NAC in protein transport, we used conditional RNA interference (RNAi)–mediated knockdown in adult animals because deletion of NAC in *C. elegans* is embryonically lethal (*13*). The knockdown of α-NAC and β-NAC, individually and in combination, substantially shortened the life span (Fig. 1A), suggesting an important function in adult *C. elegans*. Next, we used various cell compartment–specific stress reporter strains that express green fluorescent protein (GFP) under a specific stress-inducible promoter. To specifically measure cytosolic stress, we used transgenic animals carrying the *hsp-16.2p::GFP* reporter (*14*). In these worms, GFP fluorescence strongly increased upon heat shock (fig. S1A) (*15*), demonstrating the functionality of this reporter strain. Knockdown of NAC did not increase GFP expression (Fig. 1B and fig. S1B). Moreover, quantitative polymerase chain reaction (PCR) analysis of different mRNAs encoding cytosolic heat shock proteins revealed an inconsistent expression pattern. One gene was up-regulated (*hsp-70*), but the others were unaltered (*hsp-16.41* and *hsp-17*) and even down-regulated (*f44e5.4*, a member of the Hsp70 family), suggesting that NAC depletion did not cause a robust cytosolic stress response (Fig. 1F). However, depletion of NAC in animals carrying the *hsp-4p::GFP* reporter for analysis of ER stress (*16*) strongly increased GFP fluorescence (Fig. 1C and fig. S1C). Furthermore, β-NAC depletion in wild-type worms (Bristol N2) strongly induced the expression of the ER-resident chaperones Hsp-4 and Pdi-3 (Fig. 1E) and revealed enhanced *hsp-4* transcript levels as well as elevated levels of total and spliced *xbp-1* mRNA that encodes the main transcription factor of the ER stress response (Fig. 1F). Depletion of the β-NAC subunit by means of RNAi resulted in the destabilization of the α-NAC subunit (and vice versa) and thus resulted in depletion of the entire complex (Fig. 1E). Thus, NAC depletion provokes an ER stress response in adult *C. elegans*. In addition, GFP fluorescence was slightly increased in animals carrying the *hsp-6p::GFP* reporter (*17*) that specifically monitors mitochondrial stress (Fig. 1D and fig. S1D). Consistent with mitochondrial stress, we detected enhanced expression of the mitochondrial chaperone Hsp-60 in wild-type worms upon knockdown of β-NAC (Fig. 1E). Transcript levels of *hsp-60* as well as of another mitochondrial chaperone, *hsp-6*, were also significantly elevated (Fig. 1F).

Might NAC thus regulate the transport of proteins from the cytosol to the ER and mitochondria? To address this possibility, we impaired the transport pathways to these compartments by depleting the crucial targeting factors SRβ and tomm-20, respectively, and analyzed the resulting stress responses in dependence of NAC. Knockdown of β-NAC together with SRβ increased the ER stress response (Fig. 1, G and H, and fig. S2A), whereas the combined knockdown of β-NAC and tomm-20 did not provoke an enhanced mitochondrial stress response (fig. S2C). Thus, NAC has a critical function in regulating the cotranslational protein transport to the ER but seemingly does not affect the sorting of proteins to mitochondria directly. Consistent with a potential role of NAC in ER targeting, the ER stress response was also increased when β-NAC was depleted together with SRα or together with SRP54, which is an essential subunit of SRP (fig. S2, A and B).

NAC prevents SRP-independent binding of ribosomes to ER translocons

Next, we separated whole animal extracts into cytosolic and membrane fractions and investigated ribosomal particles through sucrose density gradient sedimentation analysis. As noted previously (*18*), we observed a decline of cytosolic polysome levels in β-NAC–depleted animals (Fig. 2A). Conversely, however, the levels of membrane-bound ribosomes were strongly increased, suggesting that ribosomes were redistributed from the cytosol toward the ER membrane in the absence of NAC (Fig. 2B). Consistently, immunoblot analysis also showed a clear shift of the ribosomal protein RPL-10 from the cytosol toward the membrane fraction in β-NAC–depleted animals (Fig. 2C). 12% of total ribosomes were membrane-attached in control animals, whereas in β-NAC–depleted animals, this ribosome pool increased to 31% (Fig. 2D). RNAi-mediated depletion of Sec61α—the major constituent of the ER translocon, individually and in combination with β-NAC—strongly reduced the levels of ribosomes in the membrane fraction and, concomitantly, increased them in the cytosolic fraction (Fig. 2, C and D, and fig. S3A). Because the Sec61α levels were

unaltered in β-NAC–depleted animals (Fig. 2C and fig. S3C), these data suggest that ribosomes interact to a much greater extent with ER translocons in the absence of NAC.

Next, we knocked down SRP54 to investigate whether the SRP pathway contributed to the increased binding of ribosomes to the Sec61 complex in NAC-depleted animals. As expected, SRP54 depletion shifted ribosomes from the ER membrane toward the cytosol (Fig. 2, C and D, and fig. S3B). Such ribosome redistribution did not occur in animals depleted of both β-NAC and SRP54 (Fig. 2, C and D, and fig. S3B). Because knockdown efficiencies of SRP54 and β-NAC were comparable in the single and double RNAi setups (fig. S3D), these data demonstrate that ribosomes get recruited to the ER membrane SRP-independently.

The increased, SRP-independent binding of RNCs to ER translocons suggested that ribosomes directly interact with Sec61. To test this possibility, we incubated puromycin and high salt-stripped ribosomes as well as microsomes in the presence and absence of NAC and then repurified microsomes by means of centrifugation. In the absence of NAC, ribosomes readily bound to the microsomal fraction, whereas this binding was efficiently blocked when NAC was added (Fig. 2E). The interaction of NAC with ribosomes was necessary for this blocking activity because a ribosome-binding deficient mutant of NAC, $^{RRK/AAA}$NAC (fig. S4), did not prevent binding of ribosomes to microsomes (Fig. 2E). Furthermore, we tested whether NAC also played a role in releasing ribosomes from the ER membrane after translation termination. We extracted native rough microsomes and tested the puromycin-induced release of bound ribosomes in dependence of NAC. As previously shown (*19*), treatment with puromycin only marginally released ribosomes from membranes; however, the addition of NAC strongly enhanced the puromycin-induced ribosome release, whereas $^{RRK/AAA}$NAC had no effect (Fig. 2F). Thus, NAC is a strong negative regulator of ER-transport that prevents direct, SRP-independent interactions of ribosomes with ER translocons.

NAC overexpression impairs SRP-dependent ER targeting

We reasoned that if NAC generally acts as an ER targeting inhibitor, NAC overexpression could

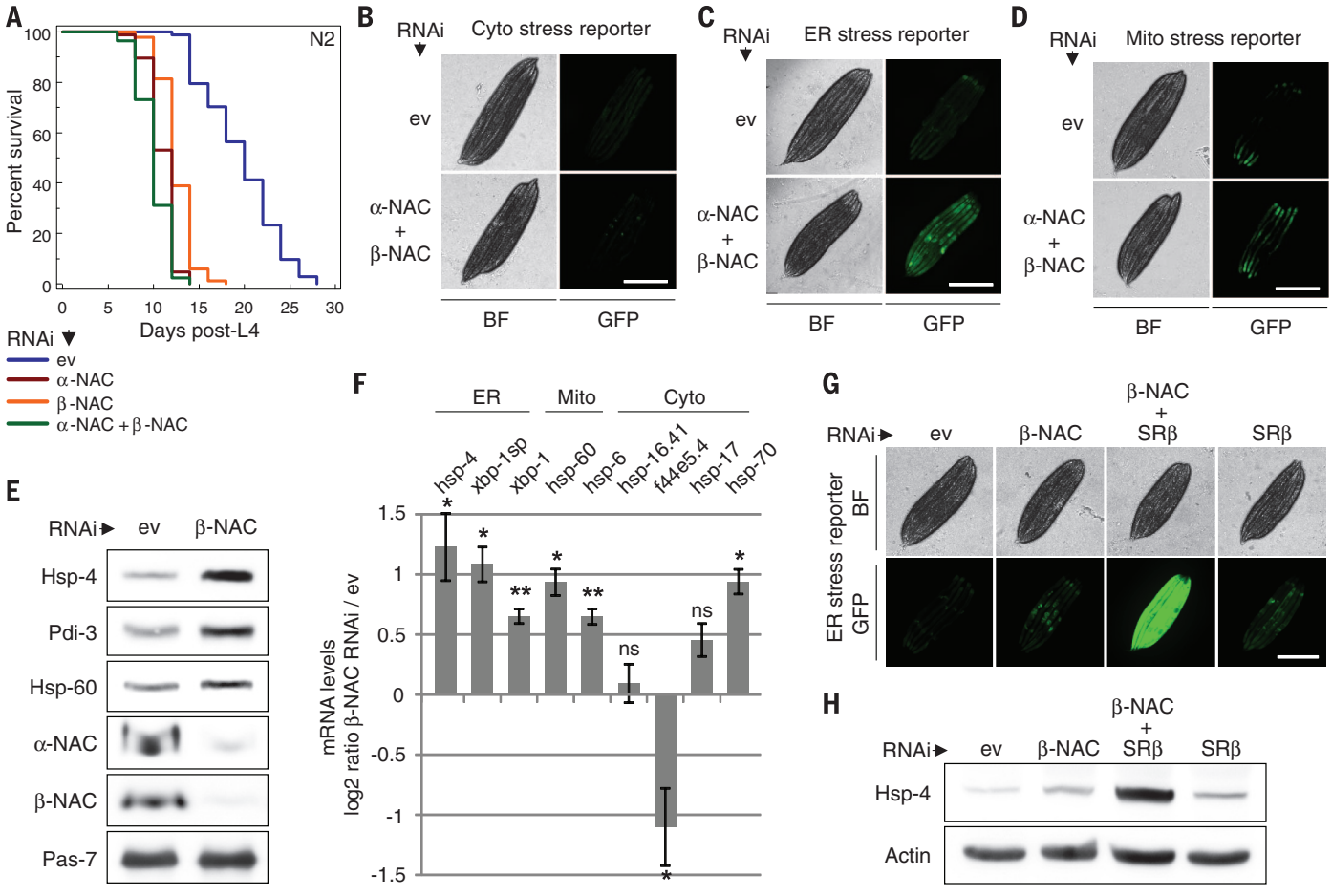

Fig. 1. NAC depletion shortens adult life span and induces stress in the ER and mitochondria. (**A**) Life span survival curves of N2 worms grown at 20°C on empty vector control (ev, blue; median life span 20 days), α-NAC RNAi (red; median life span 12 days), β-NAC RNAi (orange; median life span 12 days), or α-NAC + β-NAC RNAi (green; median life span 10 days). (**B**) *hsp-16.2p::GFP* cytosolic stress reporter worms were grown on empty vector control (ev) or α-NAC + β-NAC RNAi. GFP fluorescence was assessed on day 3 of adulthood (fig. S1, A and B). BF, bright-field. Scale bar, 0.5 mm. (**C**) *hsp-4p::GFP* ER stress reporter worms were grown on empty vector control (ev) or α-NAC + β-NAC RNAi, and GFP fluorescence was assessed on day 3 of adulthood (fig. S1C). BF, bright-field. Scale bar, 0.5 mm. (**D**) *hsp-6p::GFP* mitochondrial stress reporter worms were grown on empty vector control (ev) or α-NAC + β-NAC RNAi, and GFP fluorescence was assessed on day 2 of adulthood (fig. S1D). BF, bright-field. Scale bar, 0.5 mm. (**E**) N2 worms were grown on empty vector control (ev) or β-NAC RNAi. On day 3 of adulthood, levels of indicated proteins were assessed with immunoblotting. Immunoblot against Pas-7 served as loading control. (**F**) N2 worms were grown on empty vector control (ev) or β-NAC RNAi. On day 3 of adulthood, mRNA levels of indicated genes were assessed by means of quantitative reverse transcriptase–PCR (RT-PCR). Data are represented as mean ± SD. A Student's *t* test was used to assess significance: **P* < 0.05, ***P* < 0.01; ns, not significant. *xbp-1sp* = *xbp-1* spliced. (**G**) *hsp-4p::GFP* ER stress reporter worms were grown on empty vector control (ev), β-NAC RNAi, β-NAC + SRβ RNAi, or SRβ RNAi, and GFP fluorescence was assessed on day 2 of adulthood (fig. S2A). BF, bright-field. Scale bar, 0.5 mm. (**H**) N2 worms were grown on empty vector control (ev) or indicated RNAi. On day 2 of adulthood, Hsp-4 levels were analyzed with immunoblotting. Actin served as loading control.

interfere with the binding of ribosomes to ER translocons. We thus established transgenic animals overexpressing both NAC subunits from a strong and ubiquitous promoter (*eft-3p*). The transgenic strains showed a moderate two- to threefold overexpression of NAC (Fig. 3, C and D). All attempts to get strains with a much stronger overexpression by injecting higher amounts of DNA produced no transgenic progeny, indicating that NAC expression over a critical threshold was lethal in *C. elegans*. Consistent with this, the moderately NAC-overexpressing strains were already slightly delayed in development. The levels of cytosolic polysomes were slightly increased in NAC-overexpressing animals (Fig. 3A; quantification is provided in fig. S5A). In contrast, the levels of membrane-attached ribosomes were markedly reduced (Fig. 3B and fig. S5A). Immunoblot analysis of RPL-10 confirmed the membrane-to-cytosol shift of ribosomes, although the levels of Sec61α were unchanged (Fig. 3C). Moreover, Hsp-4 levels were significantly increased in NAC-overexpressing worms, indicating ER stress (Fig. 3D). Thus, NAC overexpression interferes with the targeting of ribosomes to ER translocons, likely by impairing the SRP pathway. To investigate this possibility, we analyzed whether NAC overexpression altered the binding of SRP to ribosomes that would be expected upon targeting inhibition. The total levels of SRP were unchanged in NAC-overexpressing animals (Fig. 3E). However, the binding of SRP to ribosomes was significantly shifted to late polysomes (Fig. 3F), indicating that new rounds of translation initiation on mRNAs encoding SRP substrates occurred in the cytosol because overexpressed NAC delayed the timely targeting of RNCs to the ER. To further explore the effects of NAC overexpression on ER targeting, we depleted critical SRP pathway components by means of RNAi in the first larval stage (L1) so as to compromise protein transport to the ER. The knockdown of SRP54, SRα, and SRβ induced developmental defects in wild-type worms that resulted in a partial larval arrest (fig. S5B). NAC-overexpressing animals were hypersensitive to these RNAi treatments (fig. S5B), whereas NAC-depleted animals were less sensitive (fig. S5C). This suggests that NAC expression above a critical threshold counteracts the activity of the SRP pathway. To corroborate this, we assessed ER targeting directly by analyzing the distribution of four ribosome-associated mRNAs encoding specific SRP substrates (*ile-2*, *sec-61*, *R186.3*, and *hsp-4*) between the cytosol and the ER membrane. As expected, knockdown of SRP54 in control animals strongly shifted these RNCs toward the cytosol (Fig. 3G). NAC overexpression strongly aggravated the targeting defects induced by SRP54 depletion (Fig. 3G). Thus, NAC may act as a general ER targeting inhibitor whose expression levels need to be accurately balanced to allow a specific derepression of ER targeting by the SRP pathway.

Global mistargeting of ribosomes to the ER in the absence of NAC

Next, we used a genome-wide microarray approach to measure the global distribution of ribosome-associated mRNAs between the cytosol and the ER membrane. Because NAC depletion in *C. elegans* results in a strongly reduced brood size (*18*), we used a temperature-sensitive sterile mutant (SS104) to minimize the risk of artifacts owing to unequal embryonic gene expression. The sterile mutants showed a NAC RNAi phenotype similar to wild-type worms (fig. S6, A to E). To test ER targeting specificity, we isolated cytosolic and membrane-attached ribosomes and quantified the translated mRNAs using DNA microarrays. The majority of mRNAs (93%) that were significantly enriched in the cytosolic fraction of control animals encoded proteins without a predicted N-terminal signal

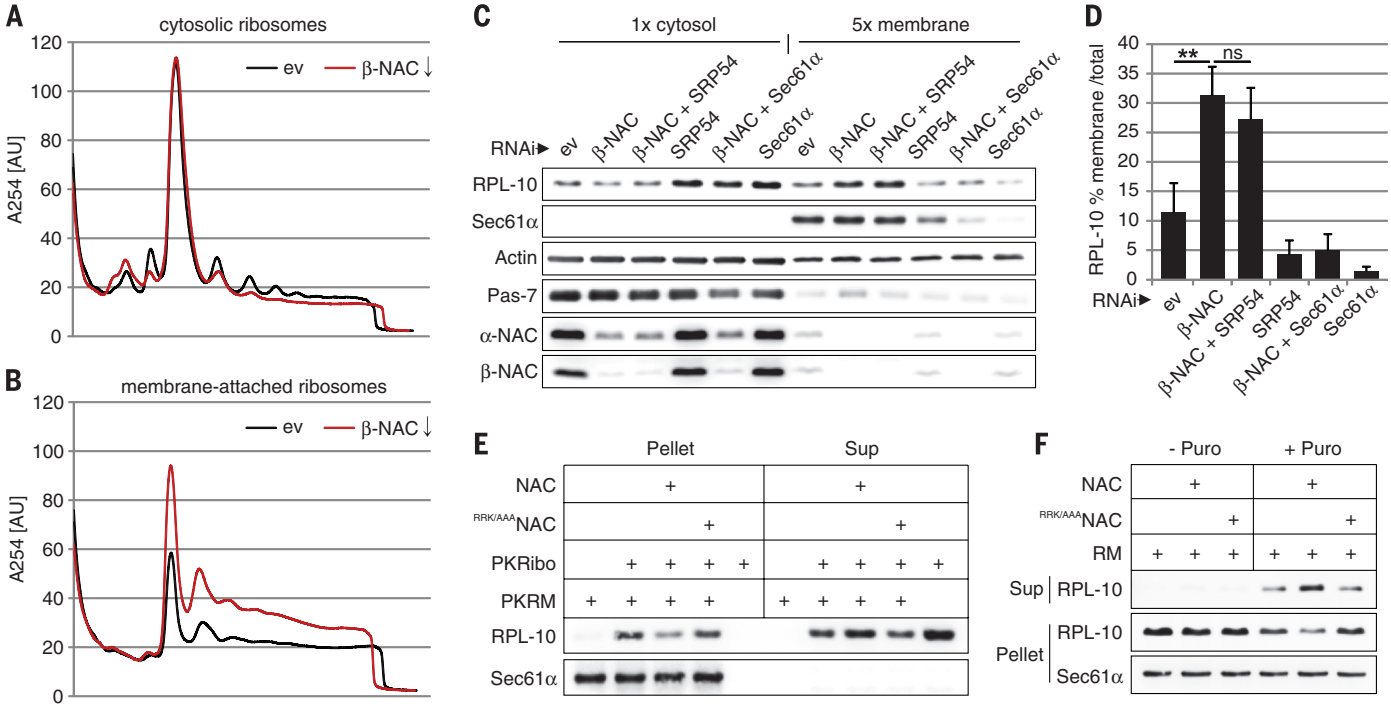

Fig. 2. NAC prevents SRP-independent ribosome-translocon binding. (**A**) Cytosolic polysome profiles of day-3 adult N2 worms grown on empty vector control (ev, black) or β-NAC RNAi (red). (**B**) Polysome profiles of membrane-attached ribosomes from animals as in (A). (**C**) N2 worms were grown on empty vector control (ev) or indicated RNAi. On day 3 of adulthood, indicated protein levels in cytosolic and membrane fractions were assessed with immunoblotting. Membrane fraction was loaded in fivefold excess over cytosolic fraction (5× membrane). Actin and Pas-7 served as loading controls (fig. S3, A and B). (**D**) Diagram shows percentage of membrane-bound ribosomes by means of RPL-10 levels in the cytosolic and membrane fractions shown as in (C). Data are represented as mean ± SD. A Student's *t* test was used to assess significance: $^{**}P < 0.01$; ns, not significant. (**E**) Puromycin and high salt-stripped ribosomes (PKRibo) and microsomes (PKRM) were incubated in the presence and absence of recombinant NAC or the ribosome-binding mutant $^{RRK/AAA}$NAC (fig. S4). Microsomes were pelleted, and bound ribosomes were analyzed by means of RPL-10 levels. Sup, supernatant. (**F**) Native rough microsomes (RM) were treated with puromycin (Puro) in the presence and absence of recombinant NAC or $^{RRK/AAA}$NAC. Microsomes were pelleted. Bound and released ribosomes were analyzed in the pellet and supernatant (Sup), respectively, with immunoblot analysis of RPL-10.

sequence or a transmembrane domain (Fig. 4A). Conversely, most mRNAs (88%) that were significantly enriched in the membrane fraction encode proteins containing a predicted N-terminal signal sequence, a transmembrane domain, or both (Fig. 4A). Thus, ER targeting in control animals was accurate, and our fractionation protocol appeared valid. We next compared the distribution of these mRNAs between control and NAC-depleted animals. Scatter plot analysis of $\log_2$-transformed mRNA ratios between membrane and cytosol revealed that the distribution of the membrane-enriched mRNAs was indistinguishable between control and NAC-depleted animals [correlation coefficient (r) = 1.0356] (Fig. 4B). However, the cytosol-enriched mRNAs were strongly shifted toward the membrane fraction in NAC-depleted worms, as evident by the lower linear regression slope (r = 0.5533) (Fig. 4B). Thus, NAC depletion does not affect the specific, SRP-mediated targeting of ribosomes to the ER membrane but induces additional unspecific binding of incorrect ribosomes. We verified these data for several mRNAs with quantitative PCR in wild-type worms. In agreement with the microarray data, mRNAs encoding nuclear, cytosolic, and mitochondrial proteins were strongly mistargeted to the ER membrane in β-NAC–depleted animals (Fig. 4C). The additional knockdown of SRP54 did not reduce the levels of these mRNAs at the ER membrane, confirming that mistargeting occurs in a SRP-independent manner. Moreover, β-NAC depletion did not alter the distribution of mRNAs encoding ER proteins, whereas knockdown of SRP54 strongly shifted these mRNAs toward the cytosol (Fig. 4C). Thus, NAC depletion does not impair the activity and specificity of the SRP pathway. The additional knockdown of β-NAC partially restored the targeting defect in SRP54-depleted worms (Fig. 4C), suggesting that in the absence of NAC ribosomes translating SRP substrates bound ER translocons in a SRP-independent manner. This explains why the larval arrest induced by impairment of the SRP pathway was significantly lower in NAC-depleted animals (fig. S5C). Furthermore, although targeting of SRP substrates was partially restored in NAC/SRP54–depleted worms, we consistently observed a further moderate increase of ribosome mistargeting (Fig. 4C). Enhanced mistargeting and at the same time less specific targeting explains why the combined depletion of NAC and essential SRP pathway components provoked such an increased ER stress response (Fig. 1, G and H, and fig. S2, A and B).

Mitochondrial proteins get mislocalized and degraded by ERAD upon NAC depletion

Knowing that a posttargeting signal sequence recognition and proofreading step takes place at the Sec61 complex (*9*), we analyzed whether or not the mistargeted ribosomes translocate their nascent chains across the ER membrane. We reasoned that potential mislocalized proteins might be degraded by the ER-associated degradation (ERAD) pathway (*20*). To enrich these substrates we depleted Sel-1, an essential component of the ERAD ubiquitin ligase complex (*21*). The knockdown of Sel-1 provoked a moderate ER stress response (fig. S7). The combined knockdown of Sel-1 and β-NAC strongly enhanced the ER stress response, which suggests that the ERAD pathway is indeed activated in NAC-depleted animals to maintain ER protein homeostasis (fig. S7). Many proteins that enter the ER lumen are *N*-glycosylated on asparagine residues in N–X–S/T sequence motifs

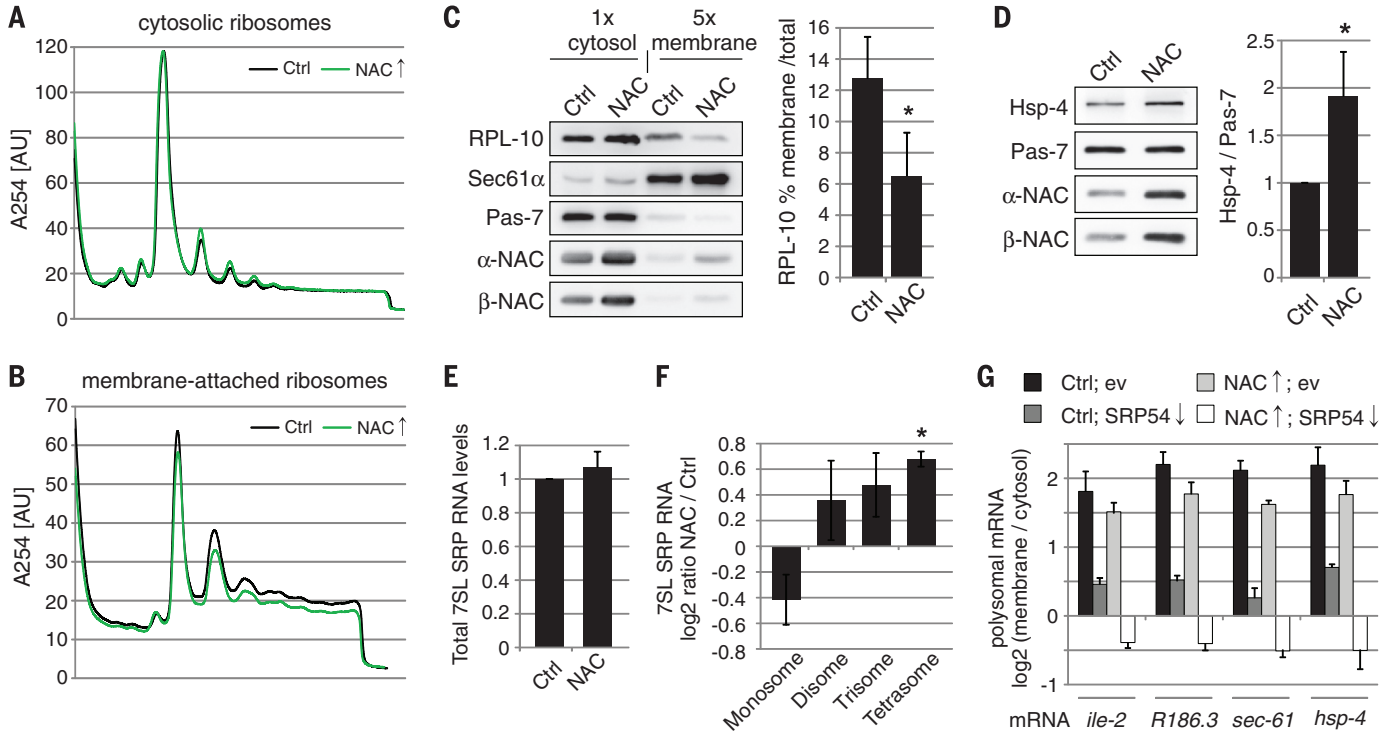

Fig. 3. NAC overexpression interferes with SRP-dependent ER targeting. (**A**) Cytosolic polysome profiles of day-2 adult control (Ctrl, black) and NAC-overexpressing worms (green). (**B**) Polysome profiles of membrane-attached ribosomes from animals as in (A). (**C**) Control (Ctrl) and NAC-overexpressing worms were harvested on day 2 of adulthood, and indicated protein levels in cytosolic and membrane fractions were assessed with immunoblotting. Membrane fraction was loaded in fivefold excess over cytosolic fraction (5× membrane). Pas-7 served as loading control. (**D**) Total extracts of animals as in (C) were prepared and indicated proteins were analyzed with immunoblotting. Pas-7 served as loading control. (**E**) Control (Ctrl) and NAC-overexpressing worms were harvested on day 2 of adulthood, and total 7SL SRP RNA levels were assessed by means of quantitative RT-PCR. Data are represented as mean ± SD. (**F**) Monosome, disome, trisome, and tetrasome fractions of ribosome sedimentation analysis shown as in (A) were collected, and 7SL SRP RNA levels were assessed by means of quantitative RT-PCR. Data are represented as mean ± SD. A Student's t test was used to assess significance: $^*P < 0.05$. (**G**) Control (Ctrl) and NAC-overexpressing worms were grown on empty vector control (ev) or SRP54 RNAi. On day 3 of adulthood, the distribution of indicated ribosome-associated mRNAs between cytosol and ER membrane was assessed by means of quantitative RT-PCR. Depicted is the $\log_2$-transformed membrane-to-cytosol ratio for indicated mRNAs. Data are represented as mean ± SD.

(*22*). We speculated that misdirected substrates containing such motifs would be *N*-glycosylated, which could be used as a footprint for mistranslocated proteins. We thus isolated glycosylated proteins using the lectin Concanavalin A (ConA) and analyzed with mass spectrometry (MS) proteins that only appeared in β-NAC/Sel-1–depleted animals. One prominent hit in the MS analysis was the mitochondrial protein Hsp-60, which contains the potential N-glycosylation site N-T-S (Fig. 5A). A substantial amount of Hsp-60 accumulated in the ConA-bound fraction of animals depleted of both β-NAC and Sel-1 (Fig. 5B). Thus, the mitochondrial protein Hsp-60 is mislocalized to the ER and degraded by ERAD in NAC-depleted animals. We then tested a second mitochondrial protein, Atp-2, that contains the predicted N-glycosylation motif N-A-S (Fig. 5A). Similar to Hsp-60, Atp-2 was also strongly enriched in the ConA-bound fraction (Fig. 5B). Treatment of the lysate with the peptide *N*-glycosidase F (PNGaseF) to remove N-glycans before the lectin affinity purification strongly diminished ConA-binding of Hsp-60 and Atp-2, corroborating that these mitochondrial proteins were indeed *N*-glycosylated (Fig. 5C). The highly abundant cytosolic protein actin (Act-1) that harbors the predicted *N*-glycosylation site N-G-S (Fig. 5A) did not accumulate in the ConA-bound fraction (Fig. 5B), although Act-1 RNCs were mistargeted to the ER translocon (Fig. 4C). This could indicate that mitochondrial targeting sequences override the proofreading function of the ER translocon pore. To analyze this more closely, we made use of a split GFP (spGFP) complementation approach (*23*). We engineered different cell compartment–specific spGFP fragments for the cytoplasm, as well as for the ER and mitochondria by fusing specific targeting sequences to spGFP (Fig. 5D). The spGFP fragments, when expressed in the same compartment, complemented only in the expected cell organelle (Fig. 5D). Animals expressing spGFP1-10 in the ER and spGFP11 in the cytosol only showed a weak background signal, and β-NAC depletion did not increase GFP fluorescence (Fig. 5E). However, knockdown of β-NAC strongly increased the GFP fluorescence in animals expressing ER-targeted spGFP1-10 and mitochondria-targeted spGFP11 (Fig. 5F). The GFP fluorescence in these worms showed a typical reticular ER pattern, revealing that the mitochondria-targeted spGFP fragments were misdirected to the ER in the absence of NAC (Fig. 5G). Thus, mitochondrial proteins in particular are incorrectly transported to the ER and subsequently degraded by ERAD. This could explain why NAC depletion induces both ER and mitochondrial stress. NAC is both an essential negative regulator for ribosome-translocon interaction to sustain ER targeting accuracy and is also important to preserve the specificity of cellular protein sorting to mitochondria.

Discussion

These findings have revealed the essential antagonistic role of NAC in regulating cotranslational protein transport to the ER. Only the combined opposing activities of SRP and NAC guarantee a robust sorting system that ensures the fidelity and specificity of protein translocation in vivo. The importance of NAC is underlined by the mistargeting of noncognate RNCs and by the fact that the in-built proofreading mechanism of the Sec61 translocon (*9*) can be overruled by mistargeted ribosomes translating mitochondrial proteins. The prevailing view has been that only nascent polypeptide chains with sufficiently hydrophobic signal sequences or transmembrane domains can open the translocation channel, whereas nonauthentic substrates would be rejected. In this work, mitochondrial targeting sequences consisting of a stretch of alternating positively charged and hydrophobic amino acid residues forming an amphipathic helix (*24*) could, at least in part, open the ER translocation channel. This is consistent with several studies showing the existence of ambiguous signals directing proteins to both mitochondria as well as the ER (*25*).

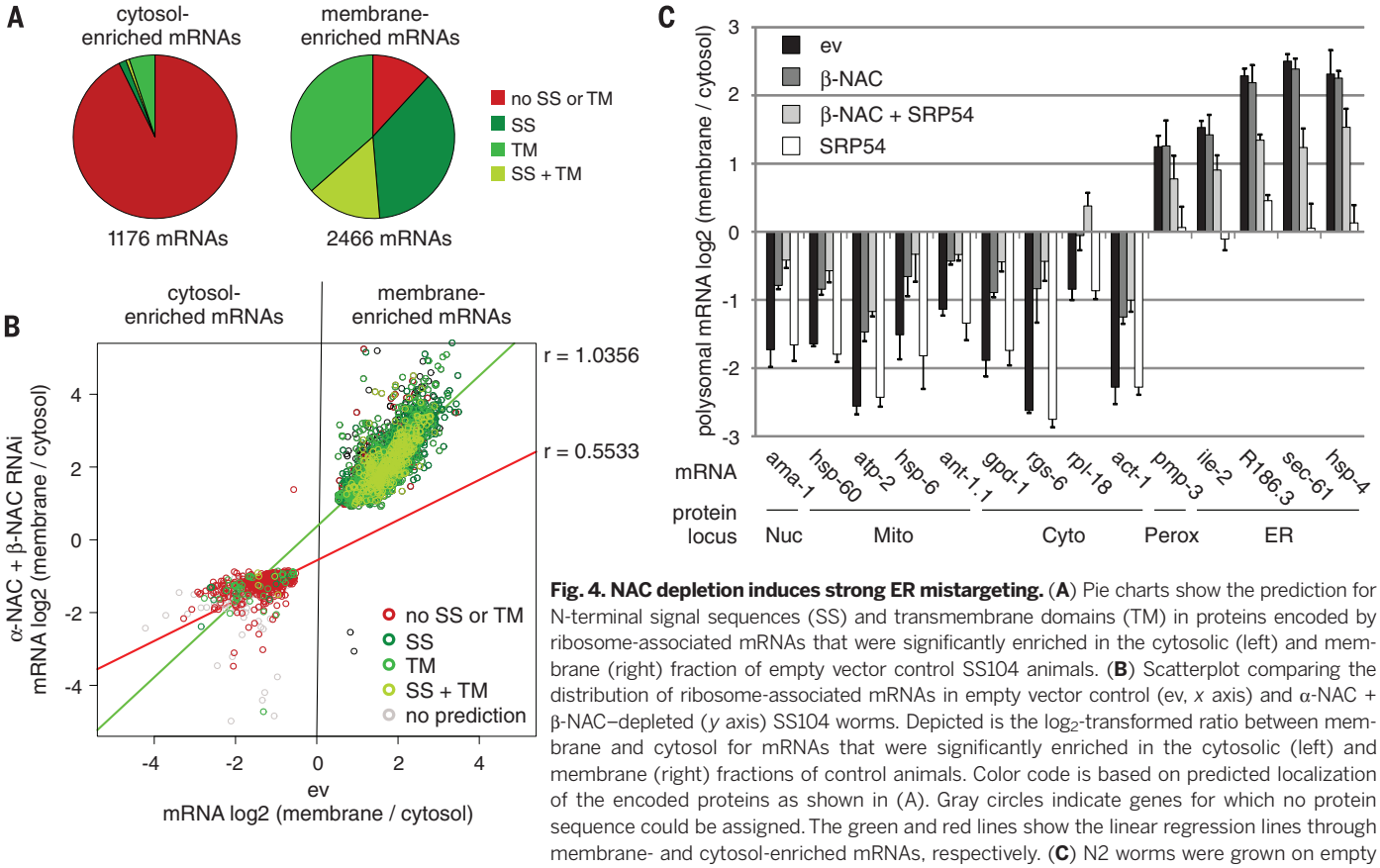

Fig. 4. NAC depletion induces strong ER mistargeting. (**A**) Pie charts show the prediction for N-terminal signal sequences (SS) and transmembrane domains (TM) in proteins encoded by ribosome-associated mRNAs that were significantly enriched in the cytosolic (left) and membrane (right) fraction of empty vector control SS104 animals. (**B**) Scatterplot comparing the distribution of ribosome-associated mRNAs in empty vector control (ev, *x* axis) and α-NAC + β-NAC–depleted (*y* axis) SS104 worms. Depicted is the $\log_2$-transformed ratio between membrane and cytosol for mRNAs that were significantly enriched in the cytosolic (left) and membrane (right) fractions of control animals. Color code is based on predicted localization of the encoded proteins as shown in (A). Gray circles indicate genes for which no protein sequence could be assigned. The green and red lines show the linear regression lines through membrane- and cytosol-enriched mRNAs, respectively. (**C**) N2 worms were grown on empty vector control (ev) or indicated RNAi. On day 3 of adulthood, the distribution of indicated ribosome-associated mRNAs between cytosol and ER membrane was assessed by means of quantitative RT-PCR. Depicted is the $\log_2$-transformed membrane-to-cytosol ratio for select mRNAs coding for proteins with destination in the nucleus (Nuc), mitochondria (Mito), cytosol (Cyto), peroxisomes (Perox), and ER. Data are represented as mean ± SD.

Our *C. elegans* study reveals that NAC counteracts the autonomous binding of ribosomes to Sec61 to ensure ER targeting specificity. A role for NAC in ER protein targeting has been indicated by several in vitro analyses (*7*, *11*, *26*). However, this hypothesis was rapidly dismissed by other in vitro studies providing contrary results (*27*, *28*). Moreover, yeast in vivo studies showed no aberrant translocation phenotype upon NAC deletion (*29*, *30*). Why the importance of NAC in ER protein targeting was missed in yeast studies is unclear. The discrepancy could be explained by the fact that yeast cells use a distinct posttranslational ER targeting system, which is seemingly not used in such a pronounced way by higher eukaryotes (*31*). Consistent with this, yeast is the only known organism in which cotranslational ER targeting by the SRP pathway is not essential (*32*). Another possible explanation for the different effects of NAC depletion in yeast and higher eukaryotes could be the potential disparate engagement of available Sec61 channels in the translocation of correct substrates. Our study in *C. elegans* reveals that NAC depletion does not impair the correct targeting of ribosomes to the ER membrane. Rather, vacant translocons that exist in adult worms become occupied by incorrect ribosomes in a SRP-independent manner. It is very likely that in yeast under optimal growth conditions most if not all translocons are saturated, thus counteracting the potential mistargeting of ribosomes occurring in the absence of NAC.

The Sec61 translocon interacts with the ribosome primarily via two cytoplasmic loops of Sec61α as well as with the N-terminal helix of Sec61γ. Both contact the ribosomal proteins uL23 and eL29 as well as the backbone of the 28*S* ribosomal RNA (rRNA) adjacent to the nascent peptide exit site (*33*). The extensive binding surfaces account for the very high inherent affinity ribosomes exhibit for the Sec61 complex (*8*, *9*, *11*). Cross-linking data suggest that NAC contacts the ribosome via the ribosomal protein uL23 (*34*). Because this ribosomal protein is also a major contact point between the ribosome and Sec61, it is very likely that NAC sterically inhibits this high-affinity translocon interaction site. However, recent studies challenge the interaction of NAC with uL23 and suggest that NAC binds to eL31 (*35*, *36*). This ribosomal protein is placed like uL23 near the tunnel exit; thus, NAC could block the functional coupling of ribosomes and translocons also via eL31. In agreement with a function as a general ER targeting inhibitor, NAC is present in equimolar concentration relative to ribosomes, it can interact with virtually all RNCs, and binds reversibly to ribosomes (*29*, *34*, *37*). The reversible binding mode allows a specific derepression of ER targeting. We propose that displacement of NAC from RNCs could be mediated by SRP that, similar to NAC, also contacts the ribosomal protein uL23 at the tunnel exit (*1*). The high affinity of SRP to hydrophobic signal sequences or transmembrane domains in nascent chains (*6*, *27*) probably gives SRP a selective advantage over NAC for ribosome binding. A competition between NAC and SRP for ribosome binding has been previously indicated by several

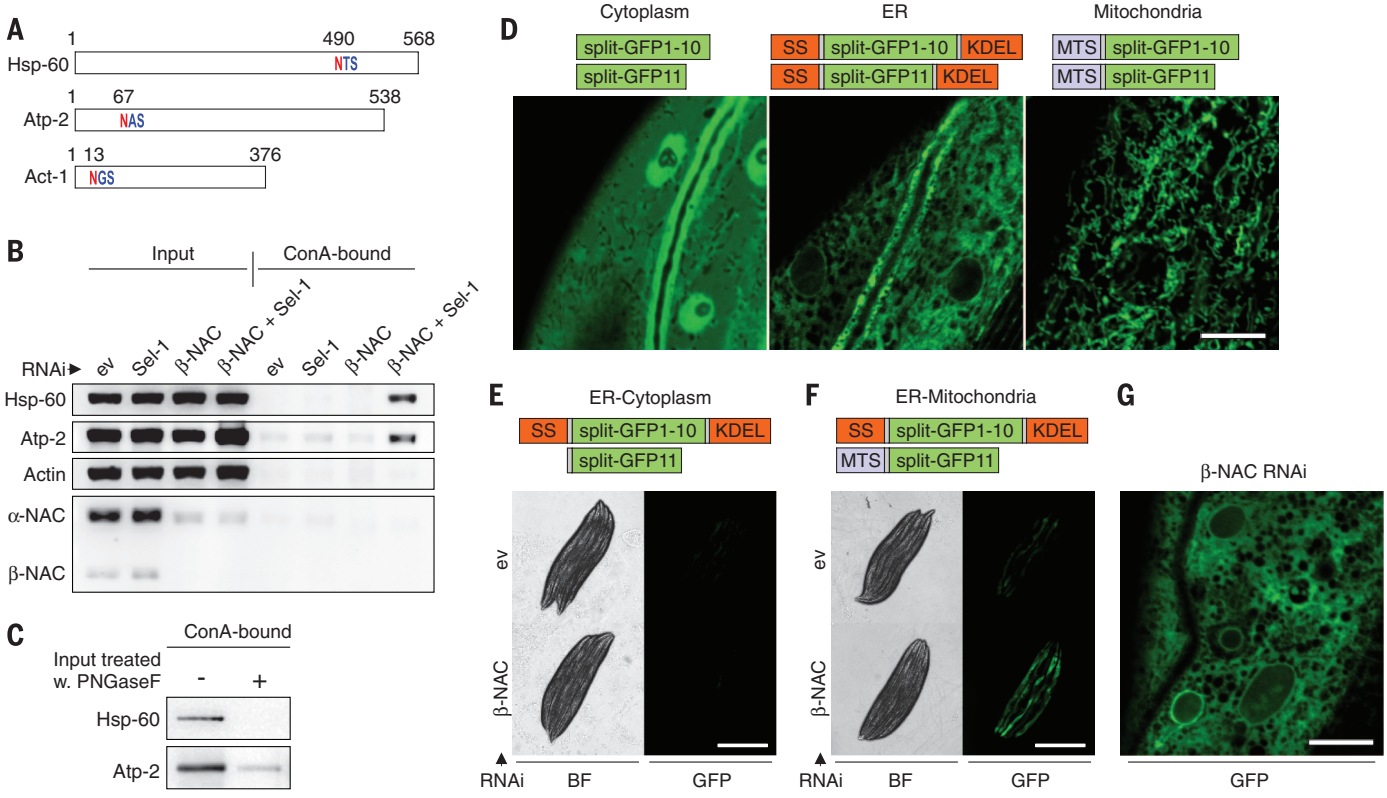

Fig. 5. Mitochondrial proteins are mislocalized to the ER and degraded by ERAD upon NAC depletion. (**A**) Schematic illustration showing predicted *N*-glycosylation sites in the mitochondrial proteins Hsp-60 and Atp-2 and the cytosolic protein Act-1. Predictions were performed with NetNGlyc 1.0. (**B**) N2 worms were grown on empty vector control (ev) or indicated RNAi. On day 3 of adulthood, glycosylated proteins were isolated by using the lectin Concanavalin A (ConA), and the levels of indicated proteins in the total extract (Input) and the lectin-bound fraction were analyzed with immunoblotting. (**C**) Total extracts (Input) of N2 worms grown on β-NAC + Sel-1 RNAi were treated or not with the *N*-glycosidase PNGaseF followed by Concanavalin A (ConA) affinity purification. The levels of ConA-bound Hsp-60 and Atp-2 were then assessed with immunoblotting. (**D**) Fluorescent micrographs of intestinal cells in worms expressing complementing split-GFP fragments in the cytoplasm (left), in the ER (middle) and in mitochondria (right). Scale bar, 10 μm. SS, ER-specific signal sequence; KDEL, ER retention motif; MTS, mitochondrial targeting sequence. (**E**) Transgenic worms expressing split-GFP1-10 in the ER and split-GFP11 in the cytoplasm were grown on empty vector control (ev) or β-NAC RNAi, and GFP fluorescence was assessed on day 2 of adulthood. BF, bright-field. Scale bar, 0.5 mm. (**F**) Transgenic worms expressing split-GFP1-10 in the ER and split-GFP11 in mitochondria were grown on empty vector control (ev) or β-NAC RNAi, and GFP fluorescence was assessed on day 2 of adulthood. BF, bright-field. Scale bar, 0.5 mm. (**G**) Fluorescent micrograph of intestinal cells in β-NAC–depleted worms as shown in (F). Scale bar, 10 μm.

in vitro studies (*26*, *36*, *38*). However, at which specific step the inhibitory action of NAC on ER targeting is counteracted by the SRP pathway is unclear.

NAC is evolutionarily conserved from yeast to man and is essential in eukaryotes, except for yeast (*13*, *30*, *39*, *40*). Knockdown of α-NAC in human HeLa S3 cells also activates ER stress responses and causes mitochondrial dysfunction (*41*). Thus, the function of NAC as an ER targeting inhibitor appears to be well conserved during evolution, at least from *C. elegans* to mammalians. Recent studies showed that NAC is sequestered by cytosolic aggregates under protein folding stress conditions (*18*, *42*). This raises the question whether proteotoxic stress in the cytoplasm causes dysfunction of NAC, leading to incorrect sorting of proteins to the ER and mitochondria. A link between cytosolic protein aggregation and ER stress is well established (*43*), and it will be interesting to investigate the role of NAC in this context.

REFERENCES AND NOTES

1. M. Halic *et al.*, *Nature* **427**, 808–814 (2004).
2. M. Halic *et al.*, *Science* **312**, 745–747 (2006).
3. Y. Nyathi, B. M. Wilkinson, M. R. Pool, *Biochim. Biophys. Acta* **1833**, 2392–2402 (2013).
4. T. A. Rapoport, *Nature* **450**, 663–669 (2007).
5. T. Schwartz, G. Blobel, *Cell* **112**, 793–803 (2003).
6. P. Walter, I. Ibrahimi, G. Blobel, *J. Cell Biol.* **91**, 545–550 (1981).
7. B. Wiedmann, H. Sakai, T. A. Davis, M. Wiedmann, *Nature* **370**, 434–440 (1994).
8. N. Borgese, W. Mok, G. Kreibich, D. D. Sabatini, *J. Mol. Biol.* **88**, 559–580 (1974).
9. B. Jungnickel, T. A. Rapoport, *Cell* **82**, 261–270 (1995).
10. K. U. Kalies, D. Görlich, T. A. Rapoport, *J. Cell Biol.* **126**, 925–934 (1994).
11. B. Lauring, H. Sakai, G. Kreibich, M. Wiedmann, *Proc. Natl. Acad. Sci. U.S.A.* **92**, 5411–5415 (1995).
12. A. Prinz, E. Hartmann, K. U. Kalies, *Biol. Chem.* **381**, 1025–1029 (2000).
13. T. A. Bloss, E. S. Witze, J. H. Rothman, *Nature* **424**, 1066–1071 (2003).
14. S. L. Rea, D. Wu, J. R. Cypser, J. W. Vaupel, T. E. Johnson, *Nat. Genet.* **37**, 894–898 (2005).
15. Materials and methods are available as supplementary materials on *Science* Online.
16. M. Calfon *et al.*, *Nature* **415**, 92–96 (2002).
17. T. Yoneda *et al.*, *J. Cell Sci.* **117**, 4055–4066 (2004).
18. J. Kirstein-Miles, A. Scior, E. Deuerling, R. I. Morimoto, *EMBO J.* **32**, 1451–1468 (2013).
19. M. R. Adelman, D. D. Sabatini, G. Blobel, *J. Cell Biol.* **56**, 206–229 (1973).
20. S. S. Vembar, J. L. Brodsky, *Nat. Rev. Mol. Cell Biol.* **9**, 944–957 (2008).
21. F. Urano *et al.*, *J. Cell Biol.* **158**, 639–646 (2002).
22. F. Schwarz, M. Aebi, *Curr. Opin. Struct. Biol.* **21**, 576–582 (2011).
23. S. Cabantous, T. C. Terwilliger, G. S. Waldo, *Nat. Biotechnol.* **23**, 102–107 (2005).
24. W. Neupert, J. M. Herrmann, *Annu. Rev. Biochem.* **76**, 723–749 (2007).
25. O. Yogev, O. Pines, *Biochim. Biophys. Acta* **1808**, 1012–1020 (2011).
26. I. Möller *et al.*, *Proc. Natl. Acad. Sci. U.S.A.* **95**, 13425–13430 (1998).
27. A. Neuhof, M. M. Rolls, B. Jungnickel, K. U. Kalies, T. A. Rapoport, *Mol. Biol. Cell* **9**, 103–115 (1998).
28. D. Raden, R. Gilmore, *Mol. Biol. Cell* **9**, 117–130 (1998).
29. M. del Alamo *et al.*, *PLOS Biol.* **9**, e1001100 (2011).
30. B. Reimann *et al.*, *Yeast* **15**, 397–407 (1999).
31. T. Ast, G. Cohen, M. Schuldiner, *Cell* **152**, 1134–1145 (2013).
32. S. C. Mutka, P. Walter, *Mol. Biol. Cell* **12**, 577–588 (2001).
33. R. M. Voorhees, I. S. Fernández, S. H. Scheres, R. S. Hegde, *Cell* **157**, 1632–1643 (2014).
34. R. D. Wegrzyn *et al.*, *J. Biol. Chem.* **281**, 2847–2857 (2006).
35. M. Pech, T. Spreter, R. Beckmann, B. Beatrix, *J. Biol. Chem.* **285**, 19679–19687 (2010).
36. Y. Zhang *et al.*, *Mol. Biol. Cell* **23**, 3027–3040 (2012).
37. U. Raue, S. Oellerer, S. Rospert, *J. Biol. Chem.* **282**, 7809–7816 (2007).
38. T. Powers, P. Walter, *Curr. Biol.* **6**, 331–338 (1996).
39. J. M. Deng, R. R. Behringer, *Transgenic Res.* **4**, 264–269 (1995).
40. D. C. Markesich, K. M. Gajewski, M. E. Nazimiec, K. Beckingham, *Development* **127**, 559–572 (2000).
41. Y. Hotokezaka *et al.*, *Cell Death Differ.* **16**, 1505–1514 (2009).
42. H. Olzscha *et al.*, *Cell* **144**, 67–78 (2011).
43. R. V. Rao, D. E. Bredesen, *Curr. Opin. Cell Biol.* **16**, 653–662 (2004).

ACKNOWLEDGMENTS

We gratefully acknowledge the help of A. Dillin and K. Steffen to get started with this *C. elegans* project. We thank the *Caenorhabditis* Genetics Center for strains and E. Schulze for the microinjection training. We also thank A. Page, W. Neupert, and C. Bargmann for providing reagents. We thank R. Schloemer, K. Turgay, C. Schlatterer, S. Zboron, and E. Oberer-Bley for their critical discussions and valuable help with the manuscript. This work was supported by research grants from the German Science Foundation (DFG; SFB969/A01) and from Human Frontier in Science Program (HFSP; RGP025) to E.D. Data are deposited in Gene Expression Omnibus under accession no. GSE63928.

SUPPLEMENTARY MATERIALS

www.sciencemag.org/content/348/6231/201/suppl/DC1
Materials and Methods
Figs. S1 to S7
References (*44*–*48*)

19 December 2014; accepted 13 February 2015
10.1126/science.aaa5335

REPORTS

QUANTUM GASES

Experimental observation of a generalized Gibbs ensemble

Tim Langen,[1] Sebastian Erne,[1,2,3] Remi Geiger,[1] Bernhard Rauer,[1] Thomas Schweigler,[1] Maximilian Kuhnert,[1] Wolfgang Rohringer,[1] Igor E. Mazets,[1,4,5] Thomas Gasenzer,[2,3] Jörg Schmiedmayer[1]*

The description of the non-equilibrium dynamics of isolated quantum many-body systems within the framework of statistical mechanics is a fundamental open question. Conventional thermodynamical ensembles fail to describe the large class of systems that exhibit nontrivial conserved quantities, and generalized ensembles have been predicted to maximize entropy in these systems. We show experimentally that a degenerate one-dimensional Bose gas relaxes to a state that can be described by such a generalized ensemble. This is verified through a detailed study of correlation functions up to 10th order. The applicability of the generalized ensemble description for isolated quantum many-body systems points to a natural emergence of classical statistical properties from the microscopic unitary quantum evolution.

Information theory provides powerful concepts for statistical mechanics and quantum many-body physics. In particular, the principle of entropy maximization (*1*–*3*) leads to the well-known thermodynamical ensembles, which are fundamentally constrained by conserved quantities such as energy or particle number (*4*). However, physical systems can contain many additional conserved quantities, which raises the question of whether there exists a more general statistical description for the steady states of quantum many-body systems (*5*).

Specifically, the presence of nontrivial conserved quantities puts constraints on the available phase space of a system, which strongly affects the dynamics (*6*–*9*) and inhibits thermalization (*10*–*12*). Instead of relaxing to steady states described by the usual thermodynamical ensembles, a generalized Gibbs ensemble (GGE) was proposed to describe the corresponding steady states via the many-body density matrix

$$\hat{\rho} = \frac{1}{Z}\exp\left(-\sum_m \lambda_m \hat{\mathcal{I}}_m\right) \qquad (1)$$

(*3*, *11*, *13*, *14*), where $\hat{\mathcal{I}}_m$ denotes a set of conserved quantities and $Z = \mathrm{Tr}[\exp(-\sum_m \lambda_m \hat{\mathcal{I}}_m)]$ is the partition function. The Lagrange multipliers λ_m associated with the conserved quantities are obtained by maximization of the entropy under the condition that the expectation values of the conserved quantities are fixed to their initial values. The emergence of such a maximum-entropy state does not contradict a unitary evolution according to quantum mechanics. Rather, it reflects that the true quantum state is indistinguishable from the maximum-entropy ensemble with respect to a set of sufficiently local observables (*5*).

[1]Vienna Center for Quantum Science and Technology, Atominstitut, TU Wien, 1020 Vienna, Austria. [2]Institut für Theoretische Physik, Ruprecht-Karls-Universität Heidelberg, 69120 Heidelberg, Germany. [3]ExtreMe Matter Institute (EMMI), GSI Helmholtzzentrum für Schwerionenforschung GmbH, 64291 Darmstadt, Germany. [4]Wolfgang Pauli Institute, 1090 Vienna, Austria. [5]Ioffe Physico-Technical Institute, 194021 St. Petersburg, Russia.
***Corresponding author. E-mail: schmiedmayer@atomchip.org**

The principle of antagonism ensures protein targeting specificity at the endoplasmic reticulum

Martin Gamerdinger *et al.*

Science **348**, 201 (2015);
DOI: 10.1126/science.aaa5335

Science (print ISSN 0036-8075; online ISSN 1095-9203) is published weekly, except the last week in December, by the American Association for the Advancement of Science, 1200 New York Avenue NW, Washington, DC 20005.